Design and construction of a DAB using SiC MOSFETs with an isolation of 24 kV for PET applications

Mariam Saeed, Maria R. Rogina, Mario López, Alberto Rodríguez, Manuel Arias, Fernando Briz
Universidad de Oviedo
Gijón, Asturias, Spain
saeedmariam@uniovi.es

Acknowledgements

This work was supported by the European Commission FP7 Large Project under grant UE-14-SPEED-604057 and by the Spanish Government under projects DPI2014-56358-JIN and the grant FPI BES-2014-070785.

Keywords

«Silicon Carbide (SiC)», «ZVS converters», «High Frequency Transformer (HFT)», « High voltage power converters», «Power electronic transformer (PET)», «Multilevel converters», «Dual Active Bridge».

Abstract

This paper analyzes the design and construction of a SiC-based Dual Active Bridge (DAB) converter for its use in a three-stage Power Electronic Transformer (PET) based on a Modular Multilevel Converter (MMC). The galvanic isolation between primary and secondary of the PET provided by the DAB High Frequency Transformer (HFT) is 24 kV. Challenges for the HFT design are discussed. A 5 kW DAB prototype using commercial 1.2–kV SiC MOSFETs is built to confirm the correctness of the design process. Parallelization of the DAB HFT to increase the power being transferred is also discussed.

Introduction

Line-Frequency Transformers (LFTs) are a mature technology. They are relatively cheap and robust, but fail to cope up with the modern grid demands. Solid State Transformers (SST), also called Power Electronic Transformers (PETs), were introduced in 1970 [1], and are considered an alternative to LFT to interface different voltage levels in the grid [2]. PET is an energy conversion system based on controllable fast-switching semiconductor devices which enables a significant reduction in volume and weight as well as fulfilling the controllability and power quality needs of emerging distributed generation grids [2], [3].

PET can be classified according to the number of stages, designs of one, two, or three stages have been proposed [4]–[7], the three-stage approach (AC/DC, DC/DC and DC/AC) appears to be the most popular choice [2], [8]–[10]. The use of Modular Multilevel Converters (MMC) at the front end (i.e. first stage AC/DC converter) is possible in this approach providing multiport capability [10]–[13].

In many applications, PET can require high isolation between its primary and secondary sides. This isolation is provided by the intermediate DC/DC stage. A Dual Active Bridge (DAB) DC/DC converter is commonly used for this role as proposed by many recent works [14]–[16]. However, in most of the works, the required isolation is not a major issue in the design mainly due to the application of interest. In this work, the selected PET topology is a modular three-stage topology based on an MMC. The HV-AC grid has a phase-to-phase voltage of 24 kV, which is the isolation required for the HFT.

A DAB converter designed to act as the intermediate DC/DC stage of a PET, and providing 24 kV of isolation through its High frequency transformer (HFT), is presented in this paper. The input and output voltages of the DAB are 800 V. SiC MOSFETs are used to comply with the high voltage and high switching frequency requirements.

The paper is organized as follows. Section II describes the selected PET topology. The SiC-based DAB converter for PET is discussed in Section III. The HFT design is presented in Section IV. Section V discuss the selection of the 1.2 kV SiC power devices. Experimental results are provided in Section VI.

PET topology description

The selected PET topology is a three-stage multiport configuration based on an MMC [12], [13], [17]–[19]. Fig. *1*-a shows a schematic of the PET topology. The MMC acts as the front end AC/DC converter providing a high-voltage AC (HVAC) and a high-voltage DC (HV-DC) links. Each MMC cell (blue) integrates a bidirectional DAB DC/DC converter (orange) to inject or drag power from the MMC cell and to provide the isolation between the primary and the secondary (see Fig. *1*-b). The outputs of all DABs are connected in parallel to provide a low-voltage (LV), high-current DC link, which is connected to the controlled rectifier (green) providing the LV-AC link.

Consequently, the considered MMC-based PET configuration provides three ports: LV-AC, HV-AC and HV-DC. The additional HV-DC port introduced by the MMC-based topology enables new functionalities compared to topologies providing only LV-AC and HV-AC ports [13].

It should be noted that the required galvanic isolation between both AC grids is provided by each DAB transformer and is not alleviated by modular design, i.e. each transformer must withstand the total peak voltage between primary and secondary. Therefore, in this specific PET topology, modularity is not an advantage from the point of view of the HFT isolation requirements as discussed previously in [18].

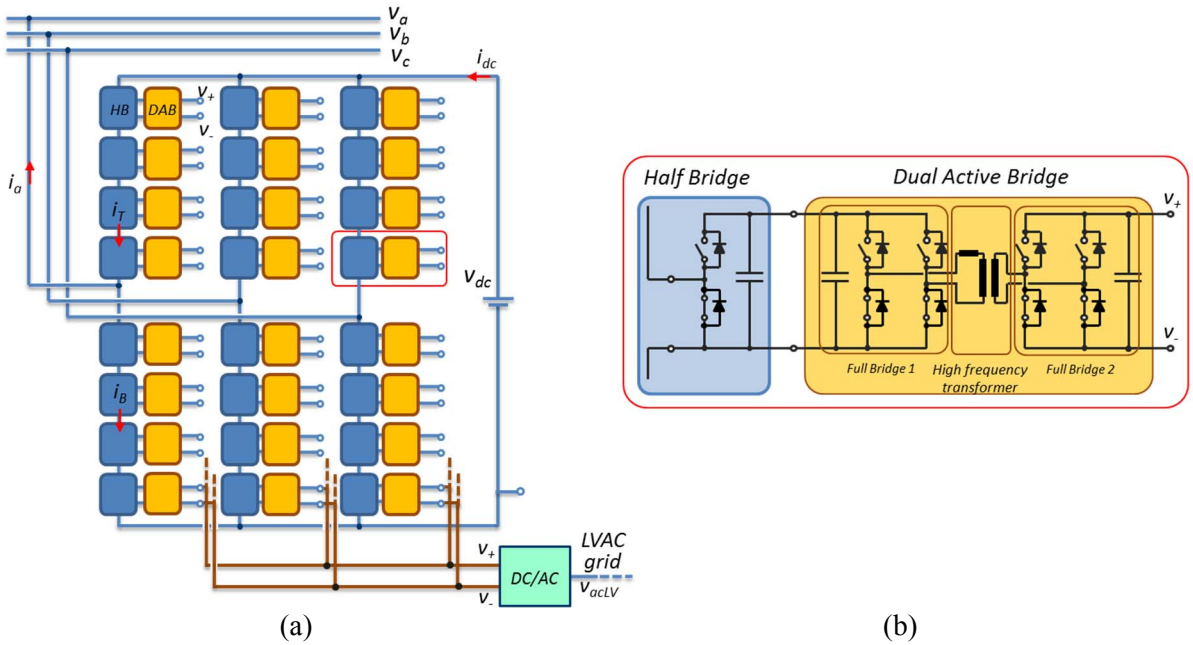

(a) (b)

Fig. 1: (a) Three-stage MMC-based PET topology. (b) Structure of one cell composed of the MMC half bridge (blue) and the DAB (orange).

Dual Active Bridge (DAB)

The DAB (see Fig. 2) is a symmetric, bidirectional DC/DC converter based on two active full bridges interfaced through an HFT. This makes it a suitable candidate for the intermediate stage of the PET, as it provides galvanic isolation through its HFT as well as realizing a bidirectional power transmission between the MMC cells and the LV side of the PET [13], [20], [21].

Both bridges are controlled with a constant duty cycle to produce a high frequency square-wave voltage at the HFT terminals. By controlling the phase shift between these square-wave voltages, a voltage difference is applied on the HFT series leakage inductance, and power is transferred from the leading bridge to the lagging one [22].

The output power delivered by the DAB P_O can be expressed by (1), where T is half of the switching period, d is the phase shift as a ratio of half a period, L_{lk} is the leakage inductance, v_O is the output voltage, v_i is the input voltage, i_O is the output current and n is the HFT turns ratio.

$$P_O = i_O \cdot v_O = \frac{(1-d)\cdot d \cdot T \cdot v_O \cdot v_i}{n \cdot L_{lk}} \quad (1)$$

This converter can have a relatively high efficiency as zero-voltage switching (ZVS) of all the devices at nominal conditions can be achieved [23].

The specifications for the DAB converter are shown in Table I. A switching frequency of 30 kHz is selected based on the tradeoff between leakage inductance value and power transfer (see (1)).

Table I: Specifications for the DAB

Parameter	Value
Rated power	5 kW
Isolation	24 kV
Switching frequency	30 kHz
RMS current	8.4 A
Input voltage	800 V
Transformer turns ratio	1 : 1
Series leakage inductance	485 uH
Transformer maximum temperature rise	60 ºC

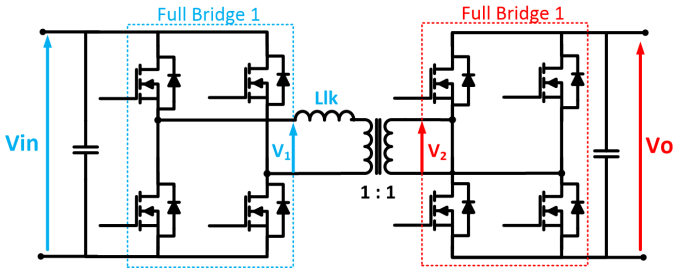

Fig. 2: Dual-Active-Bridge (DAB) converter.

High Frequency Transformer (HFT)

Targets and constraints

The HFT is one of the key components in a PET. First, it enables scaling the MMC cells voltages and the DC/AC power converter in the LV side of the PET by adequate selection of its turns ratio. It also provides galvanic isolation between the HV and LV ports of the PET, in this case 24 kV, which is considered the main challenge of this HFT design [24], [25] compared to other designs considered in the literature [26]–[28]. This high isolation implicates fixing certain design parameters related with the geometry of the transformer and consequently constraining the value of the leakage inductance as well as the temperature rise as explained in the next section.

The targets of the HFT design are shown in Table I. From (1) and the specifications shown in Table I, the required value of leakage inductance is 485 µH.

In a DAB, the leakage inductance determines the power transfer for a given switching frequency and phase shift (see (1)). Therefore, it is important to achieve an accurate value for the leakage inductance to enable working at nominal power with the nominal phase shift, thus ensuring ZVS [21]–[23]. In order to increase the power density and to reduce cost, it is advisable to magnetically integrate this series inductance as the leakage inductance of the HFT. Making use of the HFT leakage flux also makes the DAB series inductance value independent of the core and therefore independent of the core temperature

variation. However, this imposes a constraint on the design as the value of the DAB inductance will be completely dependent on the other design parameters [25].

A tradeoff must be therefore achieved between the optimization of size and losses (i.e. temperature rise) while achieving the required leakage inductance and isolation.

Design and construction

The whole HFT design is an iterative process in which isolation, temperature rise and leakage inductance requirements have to be simultaneously achieved. The process combines the use of analytical models intended to evaluate losses with Finite Element Analysis (FEA), which are used to estimate the resulting leakage inductance, temperature rise and the required isolation distances in a single magnetic component.

1. *Geometry comparative analysis:*

Three different winding structures for the HFT have been analyzed (Fig. 3): concentric, split and separate winding.

Concentric winding (see (a) in Fig. 3) can provide very low leakage inductances [26], but it is not always advantageous in a DAB application where the leakage value must be accurately selected for a certain operating point. An excessively low leakage inductance might require the use of an external inductor whose size may be comparable to the HFT, with the subsequent increase in the cost, weight and volume of the system [26]–[29]. Moreover, concentric windings configuration may compromise the maximum achievable galvanic isolation, due to the proximity of both windings. Although the required isolation may be reached, the resulting transformer design is difficult to build and not desirable therefore for industrial applications [29]. Due to this, concentric windings are disregarded.

Split windings (see (b) in Fig. 3) can achieve the required value of the leakage inductance. However, similar to the concentric design, this winding configuration compromises the maximum isolation.

Separate windings provide the required isolation but its main problem is the minimum achievable leakage inductance, as the leakage flux increases with the increase of the volume between windings. However, in this particular case, separate winding allows to integrate the required series inductance into the HFT [29]. Due to this, a configuration with separate windings was chosen finally.

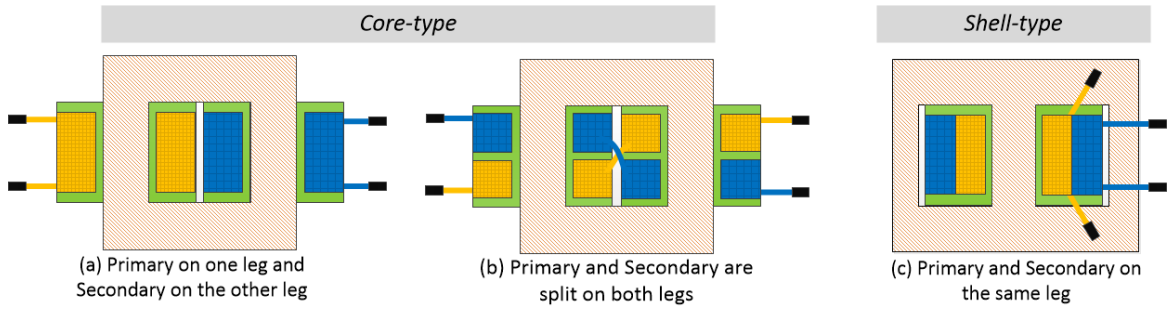

Fig. 3: The studied HFT winding structures.

2. *Core structure:*

A frequently used structure in literature is the UU core [25], [30]. The HFT is developed using two stacked UU-cores (UU100/57/25). The primary and the secondary windings are placed on separate legs of the UU-core. Ferrite material is used for the core based on the selected switching frequency (30 kHz) [26].

Both isolation between windings and between core and windings is considered. A minimum clearance distance is required between primary and secondary windings as well as between each winding and the core. These distances can be significantly decreased by encapsulating the HFT using a resin material of high dielectric strength. They are calculated based on the dielectric properties (kV/mm) of the bobbins

material (GPO3) and the encapsulation material with a safety factor of 70%. Although encapsulation is advantageous to decrease the HFT size while complying with the required isolation, it compromises the HFT core and copper temperature rise. ROYAPOX 912 THC/2 epoxy resin material was selected as it provides sufficient isolation (15 kV/mm) and good thermal conductivity (3 W/mK).

Fig. 4 shows a schematic representation of the HFT design from ANSYS PEmag®. Fig. 5-a shows the non-encapsulated laboratory developed HFT for test purposes. Fig. 5-b shows the final encapsulated HFT prototype. Isolation tests are performed using a 30 kV high potential (hipot) tester between both windings. Fig. 6 shows the experimentally measured leakage current flowing between primary and secondary windings through the air/resin versus the voltage difference between them during the isolation test for encapsulated and non-encapsulated transformers (see Fig. 5-(a) and (b)). Obviously, the encapsulated prototype shows lower leakage current between both windings, which is advantageous for high *dv/dt* to avoid very large instantaneous leakage currents leading to partial discharge and eventual isolation breakdown.

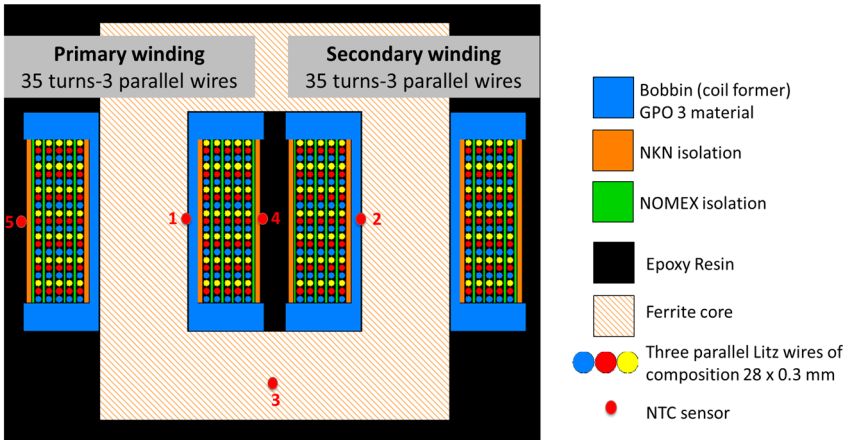

Fig. 4: HFT structure taken from ANSYS PEmag®.

(a) (b)

Fig. 5: (a) Non-encapsulated HFT laboratory prototype using two 3-D printed bobbins with 35 turns on each (b) Factory encapsulated HFT. Both designed for a rated power of 5 kW @ 30 kHz with separate windings.

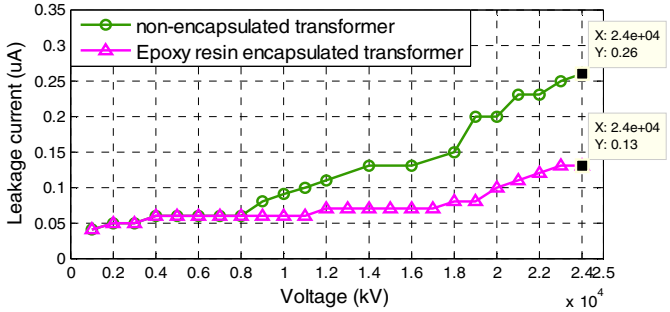

Fig. 6: Experimental results. Isolation test showing lower leakage current for the encapsulated HFT.

3. *Temperature rise*

Losses in core and copper are translated into heat, raising the temperature of the transformer, and therefore it is important to maintain this rise within acceptable limits.

Temperature rise is roughly estimated using (2) [31], where P is the sum of the winding losses and the core losses, h is the coefficient of heat transfer, A_t is the surface area and ΔT is the temperature rise. The estimated temperature rise is 40 ºC.

$$P = hA_t\Delta T \tag{2}$$

Core losses and consequently the core temperature rise strongly depends on the core material used. Three ferrite materials were tested, CF138, 3C94 and 3C90. Lab prototype is shown in Fig. 5-a. Forced air cooling is used and the temperature is measured using an NTC attached to the bare core at the hottest point, being previously identified (NTC (1) in Fig. 4). Fig. 7-a shows the temperature rise for the three materials during 3 hours of the converter operation at rated power (5 kW), 3C94 material providing the best results due to its lowest specific power loss (kW/m^3).

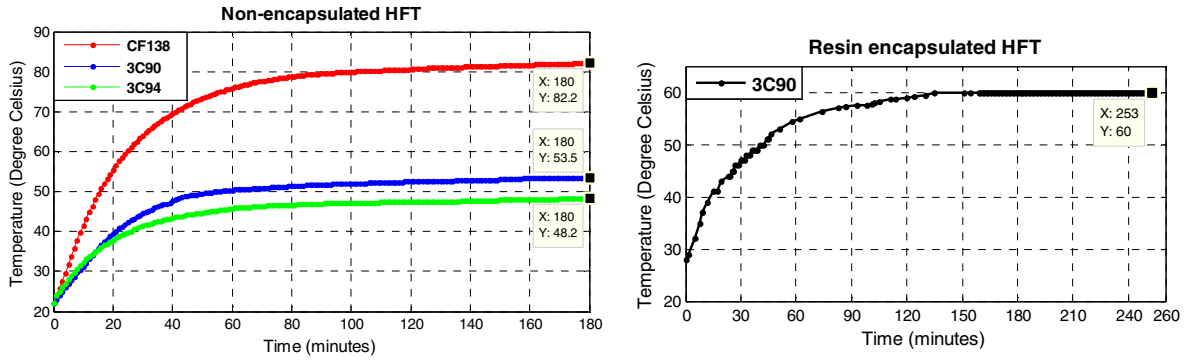

(a) (b)

Fig. 7: Experimental results. Hottest point temperature rise vs. time for (a) non-encapsulated HFT using three different ferrite materials and (b) encapsulated HFT using 3C90, both transferring 5 kW.

3C90 ferrite from Ferroxcube® was used to produce an encapsulated prototype. To confirm the correctness of the design, five NTC sensors are placed at different locations of the encapsulated HFT prototype to monitor its temperature (see Fig. 4). Fig. 7-b shows the temperature rise vs. time of the HFT hottest point during 4 hours of continuous operation of the DAB at 5 kW. The temperature rise is approximately 40 ºC with an ambient temperature of 20 ºC. This meets the target temperature (see Table II). This gives a margin of approximately 20 ºC to allow for additional temperature rise due to the closed cabinet structure.

In order to maintain the copper temperature rise within reasonable limits, the windings cable diameter and composition were calculated based on copper losses, skin effect and available window area [25]. The windings are build using three parallel litz wire of composition (28/0.5 mm) as illustrated in Fig. 4.

4. Leakage inductance

The leakage flux is mainly governed by two parameters: the volume between the windings and the number of turns. Both, higher volume and higher number of turns lead to larger leakage flux.

On one hand, the volume between both windings is constrained by the minimum isolation distances. In a separate winding transformer, this volume is difficult to calculate as it is not confined to the window volume like in the case of concentric windings and therefore it is difficult to analytically obtain a precise value for the leakage inductance.

On the other hand, the number of turns is fixed by the core and copper losses. For a fixed core structure, a theoretical optimum number of turns can be obtained which results in a minimum core and copper losses and therefore a minimum temperature rise [32].

Therefore, in this HFT design, a tradeoff is achieved between the number of turns (i.e. losses) and the value of the leakage inductance while fixing the isolation distances to the minimum required value. It is obtained using ANSYS PEmag® FEA simulations then validated by experimental measurements. The

required value of leakage inductance of 485 μH is achieved using 35 turns. The measured value from the final prototype is 435 μH.

SiC devices for the DAB

Effect of using SiC devices on the DAB

To comply with the target voltage and switching frequency (i.e. 800 V and 30 kHz), SiC MOSFETs are selected [33], [34]. Use of larger cell voltages is advantageous for the HFT design. Increasing the cell voltage for a given rated power, the required leakage inductance increases (see (1)), alleviating the problems due to long isolation distances and separate windings. It must be noted however that larger cell voltage might imply practical problems on the Auxiliary Power Supply (APS) providing the low-voltage (i.e. 24/15/12V) needed to feed the control circuitry of each cell [35].

Selection of SiC MOSFETs

Based on the DC-link voltage value (see Table I) and switching frequency, 1.2 kV SiC MOSFETs are selected. Several commercially available MOSFETs were tested in a 2-kW 400-800 V boost converter, for switching frequencies of 30, 50 and 100 kHz. The efficiency of the whole boost converter (consisting of two SiC MOSFETs) using these devices is compared.

Table II shows the results for five different options; one SiC power module as well as four different discrete N-channel SiC power MOSFET devices. It is observed from Table II that all the devices show a high efficiency. The largest dispersion occurs at 50 kHz, but is as small as 0.6 %.

Table II: SiC MOSFET Comparative Analysis

Device	Rated current (A) @100 ˚C	Rds (mΩ) @100ºC	Cout (pF)	Measured efficiency (%)		
				30 kHz	50 kHz	100 kHz
ST (SCT30N120)	34	80	130	97.77	98.16	97.81
ROHM (SCH2080KE + SBD)	28	80	175	97.71	98.02	97.69
ROHM (SCT2080KE)	28	80	77	97.82	98.17	97.93
CREE (C2M0040120D)	40	40	150	97.76	98.10	97.84
CREE module (CCS050M12CM2+ SBD)	59	25	400	97.49	97.54	97.50

Experimental results

Two devices were selected for the construction of the DAB: CREE (CCS050M12CM2) power module and ROHM (SCH2080KE) discrete power MOSFET. Two 5 kW DAB prototypes were constructed using these devices (Fig. 8-a) and efficiency is compared at rated power of the converter (i.e. 5 kW).

Commercial CREE drivers (CGD15FB45P1) were used with CREE modules CCS050M12CM2. The control signals are generated using a FPGA. Due to the high isolation requirements, the control board is divided into two sections with enough clearance to provide the 24 kV isolation. Fig. 8-b shows the measured waveforms when the DAB transfers 5 kW (see Fig. 2). The calculated efficiency of the converter from the input and output average voltages and currents is 98.5 %.

A second prototype was developed using the ROHM (SCH2080KE) discrete power MOSFET. In this case, CREE 2-channel drivers (CGD15HB62P1) are used. The efficiency of the converter is 98.1 %. The slight decrease in efficiency is attributed to the higher on-resistance of the ROHM discrete device as its rated current is relatively lower compared to the CREE module (see Table II).

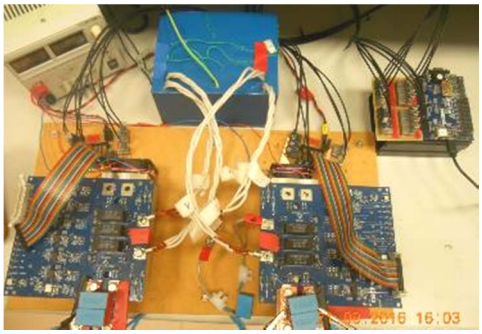

(a)

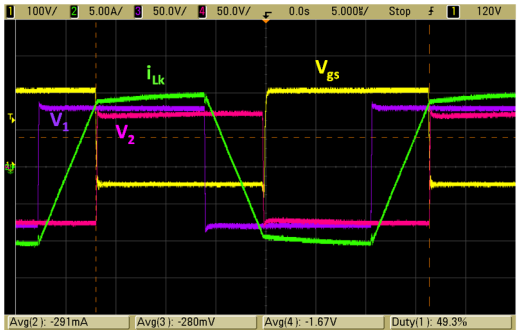

(b)

Fig. 8: (a) 5 kW DAB prototype using CCS050M12CM2 modules. (b) Experimental results. 5 kW DAB prototype waveforms. Voltage on both sides of the HFT (V_1 and V_2) and leakage inductance current (i_{LK}).

A mean to increase the power transfer while maintaining the isolation is parallelization of HFTs. To analyze this issue a DAB prototype was built with two identical HFTs connected in parallel. CREE modules CCS050M12CM2 were used. The resulting leakage inductance is 221 µH, the maximum power transferred being doubled. Fig. 9 shows the measured efficiencies for both cases: a DAB using a single HFT with a maximum power 5.7 kW and a DAB using two parallel HFTs with a maximum power of 11 kW. For both cases, the switching frequency is kept constant (30 kHz). The minimum power is limited by the DAB ZVS range while the maximum power is limited by the leakage inductance of the HFT [23]. It is observed, from Fig. 9 that increasing the power has a modest effect on the converter efficiency.

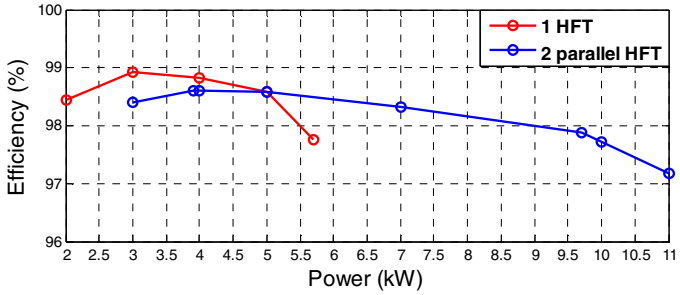

Fig. 9: Experimental results. Efficiency of the SiC DAB converter vs. transferred power at 30 kHz for two cases; (a) one HFT per DAB and (b) two HFTs in parallel per DAB.

Efficiency versus switching frequency

DAB efficiency vs. switching frequency was analyzed both analytically and experimentally. Two cases are considered: a DAB with a single HFT and with two parallel HFTs, however results are shown only for the case of two HFTs because conclusions were the same in both cases. In the case of two parallel HFTs the maximum transferable power at 80 kHz is 4 kW. It is observed from Table III that the efficiency decrease is < 0.5 % when the switching frequency increases by a factor of approximately 2.6.

Table III: SiC-based DAB converter efficiency with different switching frequencies

Switching frequency	DAB efficiency (two HFT transferring 4 kW) (%)	
	Analytical	Experimental
30 kHz	99.00	98.60
50 kHz	98.82	98.62
70 kHz	98.64	98.41
80 kHz	98.54	98.19

An estimation of the losses breakdown in the DAB between conduction, switching and HFT losses estimated analytically is shown in Fig. 10. From Table III and Fig. 10, it is observed that increasing the switching frequency by a factor of approximately 2.6 produces an increase of the switching losses of less than 15 W for a rated power of 4 kW (< 0.5%).

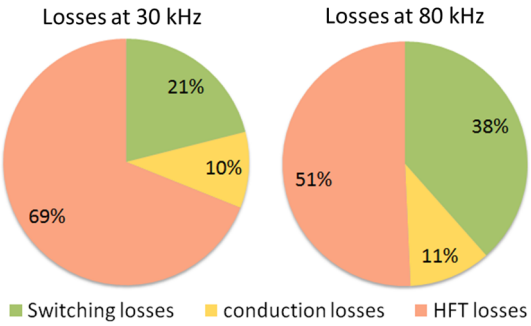

Fig. 10: Analytically estimated switching, conduction and HFT losses in the DAB at 30 and 80 kHz.

Conclusion

Design of a SiC-based DAB for a PET application has been addressed in this work. The required isolation is 24 kV which is provided by the HFT. Challenges imposed by the application on the HFT design have been discussed. These concern mainly leakage inductance, temperature rise and isolation. A 5 kW HFT, intended for a switching frequency of 30 kHz, has been built. Experimental results are shown for a DAB prototype using two different 1.2 kV SiC power devices, efficiencies as high as 98% are achieved. The measured temperature rise at the hottest point of the HFT is 40 ˚C.

Parallelization of HFTs has been proposed as a mean to increase the cell power transfer capability while complying with the high isolation requirements. This case has also been confirmed experimentally with a flat converter efficiency curve showing a slight decrease of less than 1 %. The effect of varying the switching frequency on the efficiency of the converter is analyzed. Both analytical and experimental results show a reduction of less than 0.5 % when almost tripling the switching frequency.

References

[1] W. McMurray, “Power converter circuits having a high-frequency link,” U.S. Patent 3517300, June 23, 1970.

[2] J. W. van der Merwe and H. du T. Mouton, “The solid-state transformer concept: A new era in power distribution,” in *AFRICON*, 2009, pp. 1–6.

[3] E. R. Ronan, S. D. Sudhoff, S. F. Glover, and D. L. Galloway, “A power electronic-based distribution transformer,” *IEEE Trans. Power Del.*, vol. 17, no. 2, pp. 537–543, Apr. 2002.

[4] J. Kolar and G. Ortiz, “Solid-state-transformers: Key components of future traction and smart grid systems,” presented at *the Int. Power Electronics Conf. (IPEC)*, Hiroshima, Japan, 2014.

[5] C. Zhao, D. Dujic, A. Mester, J. K. Steinke, M. Weiss, S. Lewdeni-Schmid, T. Chaudhuri, and P. Stefanutti, Philippe, “Power electronic traction transformer: Medium voltage prototype,” *IEEE Trans. Ind. Electron.*, vol. 61, no. 7, pp. 3257–3268, July 2014.

[6] M. Steiner and H. Reinold, “Medium frequency topology in railway applications,” in *Proc. European Conf. Power Electronics and Applications*, 2007, Aalborg, Denmark, pp. 1–10.

[7] S. Falcones, M. Xiaolin, and R. Ayyanar, “Topology comparison for solid state transformer implementation,” in *Proc. IEEE Power and Energy Society General Meeting*, 2010, pp. 1–8.

[8] European Union. Advanced power converter for universal and flexible power management in future electricity networks, UNIFLEX, FP6, EC Contract n: 019794 (SES6) European Commission, Directorate J-Energy.

[9] T. Zhao, G. Wang, S. Bhattacharya, and A. Q. Huang, “Voltage and power balance control for a cascaded H-bridge converter-based solid state transformer,” *IEEE Trans. Power Electron.*, vol. 28, no. 4, pp. 1523–1532, Apr. 2013.

[10] S. Xu, S. Lukic, A. Q. Huang, S. Bhattacharya, and M. Baran, “Performance evaluation of solid state transformer based microgrid in FREEDM systems,” in *Proc. 26th Annual IEEE Applied Power Electronics Conf. and Exposition (APEC)*, 2011, pp. 182–188.

[11] A. Shojaei and G. Joos, “A topology for three-stage solid state transformer,” in *Proc. IEEE Power and Energy Society General Meeting (PES)*, 2013, pp. 1–5.

[12] F. Briz, M. Lopez, A. Rodriguez, A. Zapico, M. Arias, Diaz, and D. Reigosa, "MMC-based SST," in *Proc. IEEE 13th Int. Conf. Industrial Informatics (INDIN)*, 2015, pp. 1591–1598.
[13] F. Briz, M. Lopez, A. Rodriguez and M. Arias, "Modular Power Electronic Transformers: Modular Multilevel Converter Versus Cascaded H-Bridge Solutions," *IEEE Industrial Electronics Magazine*, vol. 10, no. 4, pp. 6-19, Dec. 2016.
[14] J.W. Kolar, and J. Huber, "Solid-state transformer – key design challenges, applicability, and future concepts," *Tutorial at the Applied Power Electronics Conference (APEC)*, Long Beach, CA, USA, Mar. 20-24, 2016.
[15] Juanjuan Zhang, Yumei Du, Zixin Li and Ping Wang, "Design of a medium frequency, high voltage transformer for power electronic transformer," *IEEE Conference and Expo. Transportation Electrification Asia-Pacific (ITEC Asia-Pacific)*, Beijing, 2014, pp. 1-5.
[16] T. Parreiras, A. Machado, F. Amaral, G. Lobato, J. Brito and F. B. Cardoso, "Forward dual-active-bridge solid state transformer for a SiC-based cascaded multilevel converter cell in solar applications," *IEEE Applied Power Electronics Conference and Exposition (APEC)*, Tampa, FL, USA, 2017, pp. 2989-2996.
[17] M. Lopez, A. Rodriguez, E. Blanco, M. Saeed, A. Martinez, and F. Briz, "Design and implementation of the control of an MMC-based solid state transformer," in *Proc. IEEE 13th Int. Conf. Industrial Informatics (INDIN)*, 2015, pp. 1583–1590.
[18] M. López, F. Briz, M. Saeed, M. Arias and A. Rodríguez, "Comparative analysis of modular multiport power electronic transformer topologies," *IEEE Energy Conversion Congress and Exposition (ECCE)*, Milwaukee, WI, 2016, pp. 1-8.
[19] "Silicon Carbide Power Technology for Energy Efficient Devices (SPEED)", Ref. FP7-NMP3-LA-2013-604057, EU– FP7, Large Scale Integrating Collaborative Research Project.
[20] R. W. De Doncker, R. W. Divan, and M. H. Kheraluwala, "A three-phase soft-switched high power-density dc/dc converter for high-power applications," *IEEE Trans. Ind. Appl.*, vol. 27, no. 1, pp. 63–73, Jan. 1991.
[21] M. H. Kheraluwala, R. W. Gascoigne, D. M. Divan, and E. D. Baumann, "Performance characterization of a high-power dual active bridge dc-to-dc converter," *IEEE Trans. Ind. Appl.*, vol. 28, no. 6, pp. 1294–1301, Nov. 1992.
[22] A. Rodríguez, J. Sebastian, D. G. Lamar, M. M. Hernando, and A. Vazquez, "An overall study of a dual active bridge for bidirectional DC/DC conversion," in *Proc. IEEE Energy Convers. Congr. Expo.,* pp. 1129–1135, Sep. 2010.
[23] A. Rodríguez, A. Vázquez, D. G. Lamar, M. M. Hernando and J. Sebastian, "Different Purpose Design Strategies and Techniques to Improve the Performance of a Dual Active Bridge With Phase-Shift Control," *IEEE Transactions on Power Electronics*, vol. 30, no. 2, pp. 790-804, Feb. 2015.
[24] Z. Ouyang, J. Zhang and W. G. Hurley, "Calculation of Leakage Inductance for High-Frequency Transformers," *IEEE Transactions on Power Electronics*, vol. 30, no. 10, pp. 5769-5775, Oct. 2015.
[25] G. Ortiz, J. Biela and J. W. Kolar, "Optimized design of medium frequency transformers with high isolation requirements," *IECON - 36th Annual Conference on IEEE Industrial Electronics Society*, Glendale, AZ, 2010, pp. 631-638.
[26] M. Mu, L. Xue, D. Boroyevich, B. Hughes and P. Mattavelli, "Design of integrated transformer and inductor for high frequency dual active bridge GaN Charger for PHEV," *IEEE Applied Power Electronics Conference and Exposition (APEC)*, Charlotte, NC, 2015, pp. 579-585.
[27] K. D. Hoang and J. Wang, "Design optimization of high frequency transformer for dual active bridge DC-DC converter," *international Conference on Electrical Machines Electrical Machines (ICEM)*, Marseille, 2012, pp. 2311-2317.
[28] H. Chen and D. Divan, "High-frequency transformer design for the soft-switching solid state transformer (S4T)," *IEEE Applied Power Electronics Conference and Exposition (APEC)*, Tampa, FL, USA, 2017, pp. 2534-2541.
[29] Y. Du, S. Baek, S. Bhattacharya and A. Q. Huang, "High-voltage high-frequency transformer design for a 7.2kV to 120V/240V 20kVA solid state transformer," *IECON - 36th Annual Conference on IEEE Industrial Electronics Society*, Glendale, AZ, 2010, pp. 493-498.
[30] S. Zhao, Q. Li and F. C. Lee, "High frequency transformer design for modular power conversion from medium voltage AC to 400V DC," *IEEE Applied Power Electronics Conference and Exposition (APEC)*, Tampa, FL, USA, 2017, pp. 2894-2901.
[31] W. G. Hurley, W. H. Wolfle and J. G. Breslin, "Optimized transformer design: inclusive of high-frequency effects," *IEEE Transactions on Power Electronics*, vol. 13, no. 4, pp. 651-659, Jul 1998.
[32] S. Zhao, Q. Li and F. C. Lee, "High frequency transformer design for modular power conversion from medium voltage AC to 400V DC," *IEEE Applied Power Electronics Conference and Exposition (APEC)*, Tampa, FL, 2017, pp. 2894-2901.
[33] Peter Friedrichs, "Silicon Carbide power devices - Status and upcoming challenges," *Power Electronics and Applications*, European Conference, Sep. 2007, pp. 1 – 11.
[34] J. Millán, P. Godignon, X. Perpiñà, A. Pérez-Tomás and J. Rebollo, "A Survey of Wide Bandgap Power Semiconductor Devices," *IEEE Transactions on Power Electronics*, vol. 29, no. 5, pp. 2155-2163, May 2014.
[35] A. Rodriguez et al., "Auxiliary power supply based on a modular ISOP flyback configuration with very high input voltage," *IEEE Energy Conversion Congress and Exposition (ECCE)*, Milwaukee, WI, 2016, pp. 1-7.